Development of a novel laser range scanner

Thomas S. Pheiffer[a], Brian Lennon[b], Amber L. Simpson[a], Michael I. Miga[a]

[a]Vanderbilt University, Department of Biomedical Engineering, Nashville, TN 37235
[b]Pathfinder Therapeutics, Inc., Nashville, TN 37204

ABSTRACT

Laser range scanning an organ surface intraoperatively provides a cost effective and accurate means of measuring geometric changes in tissue. A novel laser range scanner with integrated tracking was designed, developed, and analyzed with the goal of providing intraoperative surface data during neurosurgery. The scanner is fitted with passive spheres to be optically tracked in the operating room. The design notably includes a single-lens system capable of acquiring the geometric information (as a Cartesian point cloud) via laser illumination and charge-coupled device (CCD) collection, as well as the color information via visible light collection on the same CCD. The geometric accuracy was assessed by scanning a machined phantom of known dimensions and comparing relative distances of landmarks from the point cloud to the known distances. The ability of the scanner to be tracked was first evaluated by perturbing its orientation in front of the optical tracking camera and recording the number of spheres visible to the camera at each orientation, and then by observing the variance in point cloud locations of a fixed object when the tracking camera is moved around the scanner. The scanning accuracy test resulted in an RMS error of 0.47 mm with standard deviation of 0.40 mm. The sphere visibility test showed that four diodes were visible in most of the probable operating orientations, and the overall tracking standard deviation was observed to be 1.49 mm. Intraoperative collection of cortical surface scans using the new scanner is currently underway.

Keywords: laser range scanner, neurosurgery, image-guided surgery

1. INTRODUCTION

A current area of research in the field of image-guided surgery (IGS) is deformation tracking and model-updated IGS. The primary objective of this research is the enhancement of current IGS navigation with intraoperative information on soft tissue deformation provided to update preoperative images. Accounting for this deformation is important in neurosurgery, as it has been observed that the brain can experience significant shift during the procedure[1, 2], and thus quickly degrades guidance fidelity. Even at the earliest stages, it has been observed that the brain can experience shift, which necessitates a method of monitoring this shift throughout the operation[3, 4].

One method to both align image-to-physical space as well as track deformations is through the use of a laser range scanner (LRS). In the case of registration, the cortical surface may be captured intraoperatively with the LRS and registered to preoperative images[5-7]. Miga *et al.* demonstrated an initial implementation of an organ-based registration method in which textured LRS data of the cortical surface was registered to its corresponding grayscale MR image[6]. Sinha *et al.* deployed an LRS clinically in an eight-patient preliminary study to compare several forms of cortical surface registration[7]. Cao *et al.* conducted a more comprehensive evaluation of image-to-physical registration methods for image-guided neurosurgery, including both extracranial and intracranial methods[8]. In the case of deformation measurements, a series of range scans has been used to track deformation[9-11]. For example, Sinha *et al.* used the texture associated with the point clouds to nonrigidly register them, thus providing measurements of brain shift. The accuracy of LRS data has been adequate for these purposes in the past, but improvements to conventional LRS design were identified which may increase fidelity and ease of use.

LRS designs that allow for field-of-view colored point clouds usually call for a two-lens system in which one lens captures geometric data via a laser, and the other lens captures color information via a digital camera. Unfortunately, the use of separate lenses requires additional calibration to map the 2D color information onto the 3D scanner point cloud. In

this work, this limitation is overcome with the single-lens LRS design presented here. This novel LRS design is implemented and evaluated with the intent to use in cortical surface tracking.

2. DESIGN AND DEVELOPMENT

This paper reports the results of a collaborative effort to design a new laser range scanner capable of capturing geometric and field-of-view color information using a single-lens solution. Working with Pathfinder Therapeutics Inc. engineers (Nashville, TN – www.pathsurg.com), the single-lens solution is unique in that existing solutions that capture both geometric and color information typically require two lenses and two CCDs. In addition to increasing overall cost, the overlay of color information onto the scan data is an additional source of error, as each lens will impart a unique geometric distortion on the scene being observed, and each lens has a different field of view of the target. One approach considered was to use two CCDs fed by a beam splitter connected to a single lens. The added cost, size, and complexity made this option less desirable than a single CCD solution. For the single-CCD solution described, a Basler Pilot camera (Basler Vision Technologies, Ahrensburg, Germany) running at 1920x1080@32 fps was chosen. Since this camera is part of a family of cameras with identical physical dimensions and electrical interfaces, other models from this series can be chosen based on scanning accuracy and speed requirements.

In order to image the target object, a red laser (with wavelength 635 nm) with a uniform line generator was selected. This wavelength was chosen due to both the availability of diode modules as well as its known reflectivity on the organs of interest. One drawback to the red laser is that the Bayer color filter pattern (which filters pixels to record color as either red, green, or blue before interpolation generates the final image) used on the CCD only assigns one out of every four pixels to capture red light, thereby reducing the effective resolution of the scanner. There was consideration given to using a green laser, since the Bayer pattern assigns two out of every four pixels to green, but in some intended applications this would result in a reduction of laser contrast to the background image.

The laser line is swept across the surface of the target object using a mirror attached to a galvanometer. The galvanometer chosen is capable of approximately 15-bit precision over a mechanical rotation of 40°, with a settling time in the neighborhood of 0.1 ms. With a video frame rate of 32 Hz, the maximum exposure length at that rate is 31.25 ms. By utilizing the small window of time when the CCD is shifting data out to the frame buffer and no longer collecting photons, the galvanometer is allowed to settle at its next resting position during this otherwise unutilized time period.
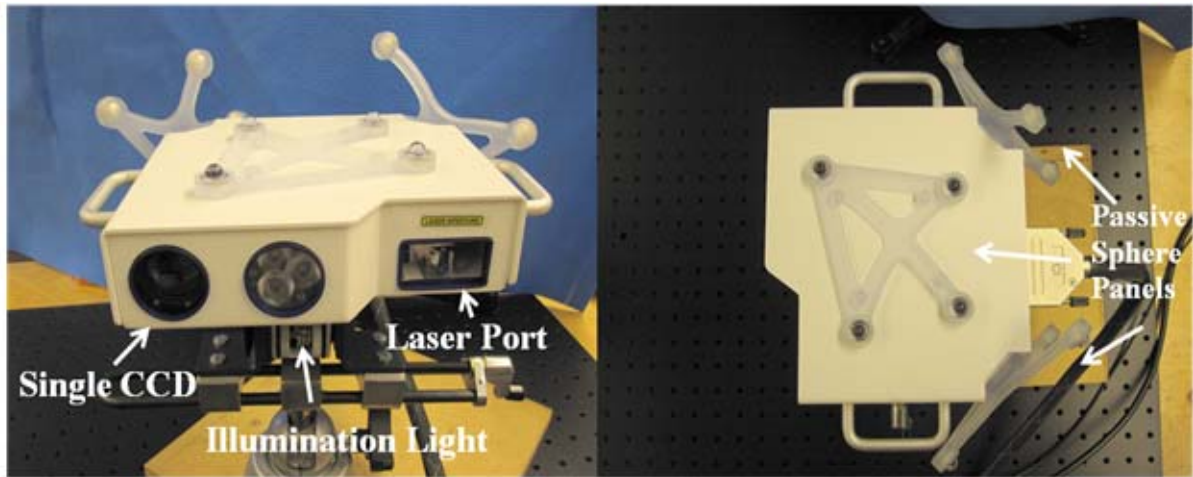
Figure 1. The novel LRS, showing the single CCD design from the front (left picture) and the tracking sphere configuration from the top of the scanner (right picture).

In order to achieve the fastest possible scans, the full frame rate of the CCD is used. Using 8-bits per pixel, the CCD will output data at a rate of 531Mb/s. In the past, this high data rate would point to a digital signal processor (DSP) based processing solution, so that the relatively low rate point cloud could be calculated in the scanner and transmitted to the host PC upon completion of the scan. Taking advantage of modern-day CPUs and reliable high-speed communications

links, the raw video frames are transferred to the host PC via Gigabit Ethernet for processing (namely correction, filtering, and detection).

The size of the enclosure was chosen to be as small as possible to accommodate the following hardware: camera, lens, white-light illuminator, galvanometer, galvanometer driver board, motherboard containing the microcontroller with support circuitry, and tracking spheres (see Figure 1). Within the enclosure, an internal structure was created to hold the camera, laser, and galvanometer perfectly rigid to each other, as even slight changes in their relative positions would invalidate the scanner calibration. The calibration process and fixture are proprietary in nature, but it can be stated that it is a semi-automated process whereby the scanner is trained on how to measure distance, determine various optical parameters specific to the hardware used, correct for geometric distortions, and other similar functions. Significant effort was placed on this calibration process to extract the maximum performance out of the hardware as well as reduce the requirements for strict manufacturing tolerances on custom fabricated hardware, such as the enclosure and optical bench.

Lastly, the tracking electronics were originally designed to be compatible with the NDI Certus position sensor (Northern Digital Inc., Waterloo, ON, Canada). The first design included small infrared diode pods that were the same height as the scanner enclosure. Testing indicated that the error in properly triangulating the position of these diodes was too great, so enlarged diode housings were constructed and tested. The design and connection of the diode housings was chosen such that they could be replaced easily, without making modifications to the scanner enclosure itself. One variation already realized is replacing the infrared diode housings with the reflective sphere panels compatible with the NDI Polaris Spectra position sensor for passive tracking. The passive configuration is currently preferred in our work, as it eases the process of integrating our hardware into existing workflow in the operating room by removing the wires of the actively-tracked diodes (the biggest impact being the reference target, which must be rigidly attached to the patient via the bed).

3. METHODS

The efficacy of the LRS was analyzed in two tests. The first was to evaluate the accuracy of the geometric range scans. A multi-level platform phantom was generated and machined such that the distances between disk centers were known within 0.05 mm relative to each other (see Figure 2, right). The phantom was first used to determine the effective work volume of the scanner based upon the ability of the laser to generate a scan of the phantom as it was passed over it. The work volume was determined to be approximately 0.3 m x 0.3 m x 0.3 m, such that the center of the work volume cube was located approximately 0.5 m away from the scanner lens. Data collection for the geometric accuracy test consisted of positioning the LRS horizontally on an optical breadboard platform pointing at the phantom and acquiring multiple scans of the phantom. The LRS was kept completely stationary, whereas the phantom was moved systematically through the work volume and scanned at each position. Nine positions in the work volume were used, consisting of three positions on each of three planes (see Figure 2, left) such that at least six disks were visible in an individual scan (several disks were not visible in the non-central positions due to field of view limitations). From the point clouds, the geometric centroid of each disk at each position was calculated. Then at each position, the relative distances between centroids were compared to the known disk distances based on the machined phantom and error statistics were calculated.
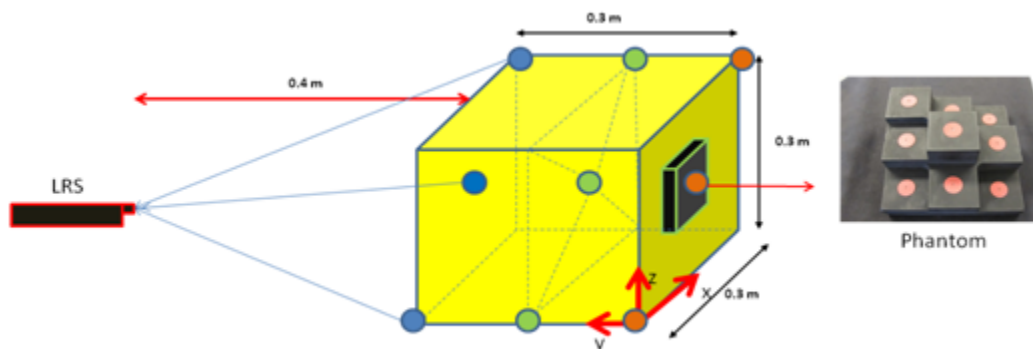
Figure 2. Geometric accuracy test setup (left) showing the nine positions of the machined phantom (right).

The second test was an observation of the tracking ability of the LRS. The first part of this test was to observe the tracking behavior of the scanner. The rigid body file describing the LRS passive sphere configuration was formulated by characterizing the LRS as a passive three-face tool in the NDI software. Each face consisted of four of the twelve markers, divided into the planes formed by the rear and top panels, respectively (see Figure 1). The visibility of the spheres was tested by placing the Polaris camera and the LRS in "typical" operating room positions. The Polaris was mounted horizontally at a height of approximately 2 m, whereas the LRS was mounted at a height of 1 m at a horizontal distance of 1.5 m directly in front of the Polaris. Keeping the positions of the Polaris and the LRS constant, the orientation of the LRS was incremented via its pitch (φ) and yaw (θ) as shown in Figure 3 to simulate plausible orientations in the operating room. The pitch was set to 0, 45, and 90° with respect to the floor. At each pitch, the yaw was incremented by 30° through a full 360° rotation and the number of spheres tracked was recorded via NDI First Principles tracking software.
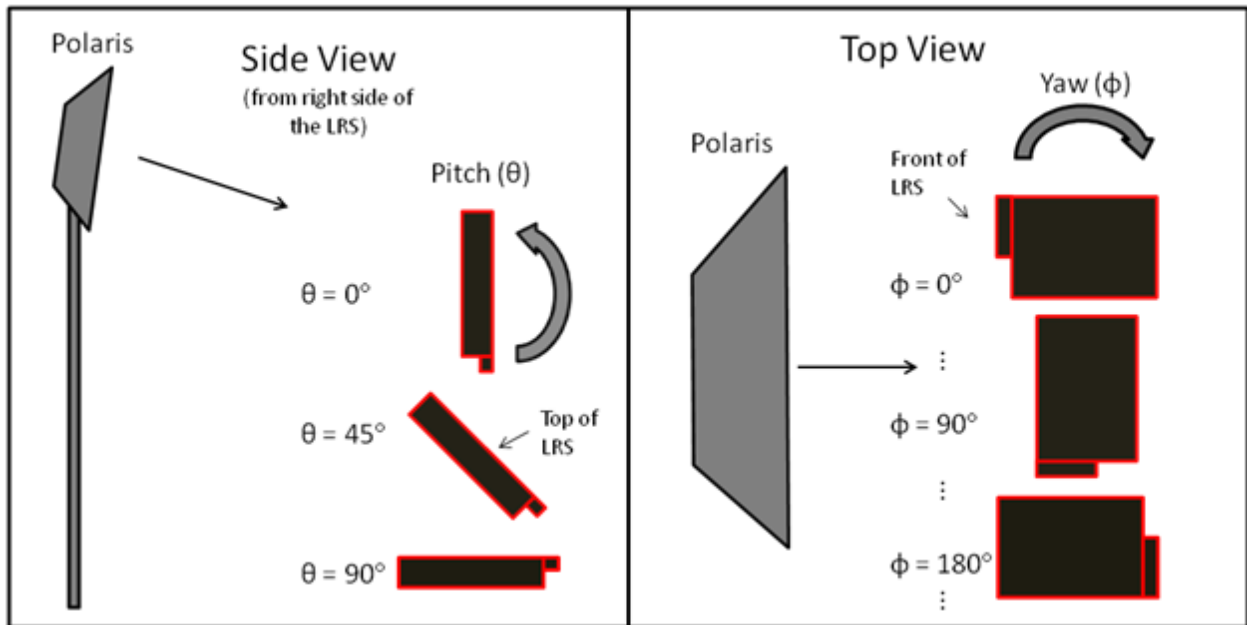
Figure 3. Orientations used in sphere visibility test. For reference, a pitch of 0° and a yaw of 0° denotes the LRS being oriented vertically with its top facing toward the Polaris, whereas a pitch of 90° and yaw of 180° denotes a horizontal orientation facing away from the Polaris.

The second tracking test was conducted to observe the robustness of the rigid body file description. First, the transformation from "point cloud space" to "reference target space" is determined via a standard least-squares calibration procedure. The calibration is done by scanning the machined block phantom from above, and then determining the centroids of the discs in the point clouds. An optically-tracked pen probe is then used to determine the location of the disc centroids in camera space. The scan centroid points are fitted to the probe points in order to generate a 4x4 calibration matrix which transforms scan points into the space of the reference target. The scanner was calibrated this way three times (once while tracking each face) and the three calibration matrices were averaged to arrive at an overall calibration.
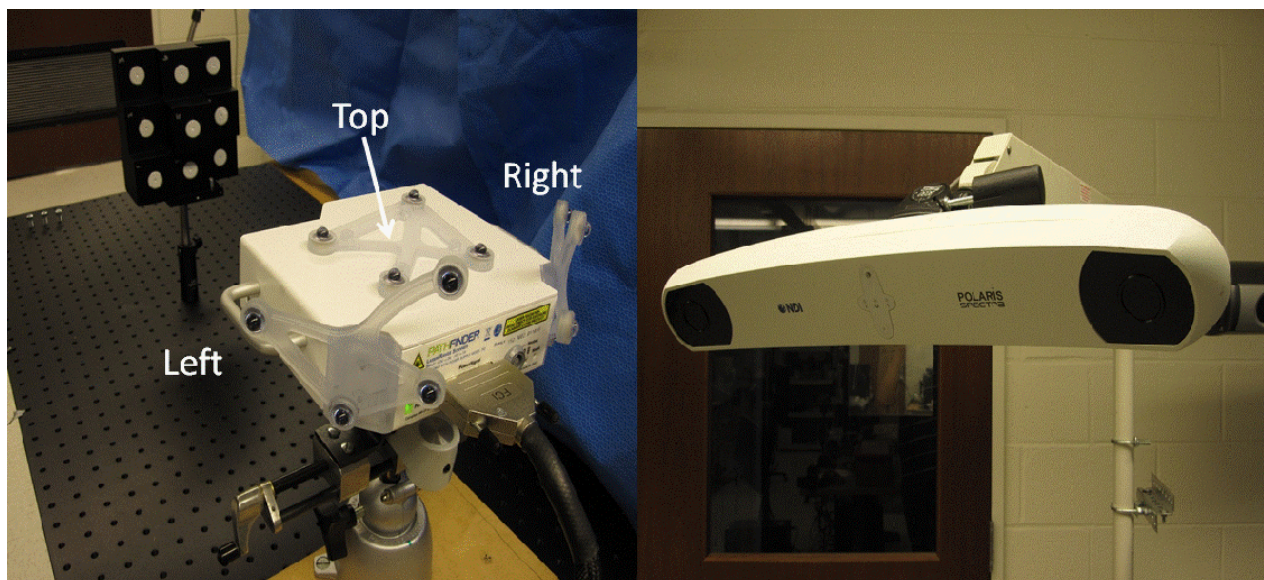
Figure 4. Setup of the fixed LRS and phantom on the optical breadboard (left) used for the tracking test, as well as the Polaris sensor (right) used to track the LRS.

After generating this calibration, the LRS was positioned horizontally facing the block phantom, which was placed in the center of the LRS work volume. Both objects were fixed in place as shown above in Figure 4, and the reference target was placed next to the block phantom. In this test, the Polaris camera was moved between 30 positions that were distributed approximately 360° around the LRS, such that the Polaris tracked each of the three sphere panels for ten of the scans, respectively. At each position of the camera, a scan of the phantom was acquired with the LRS and the disc centroids were determined and mapped into the space of the reference target. The average 3D standard deviation of the centroid points was calculated as a measure of how well the LRS rigid body is tracked. In addition, the mean centroid positions of the nine discs were calculated from all 30 scans, and these mean coordinates were designated as the "gold standard" coordinates for the centroids. Then the three subsets of 10 scans were compared to the gold standard centroid coordinates, and a mean difference and standard deviation was calculated for each panel.

4. RESULTS

The results of the geometric accuracy test are shown below in Table 1. The number of data points, n, was 1980 due to the combinations of relative centroid distances over the trials, minus any contribution from non-visible disks due to field-of-view issues.

Table 1. Disk centroid error statistics.

RMS error	0.47 mm
Mean error	0.37 mm
Std. Dev.	0.40 mm
Max	1.58 mm

The sphere visibility test revealed that in all of the tested orientations except for one (which was the orientation with the LRS positioned vertically with its top facing away from the Polaris, i.e. a pitch of 0° and yaw of 180°) that the NDI sensor was able to track at least one of the four-sphere faces. It should be noted that the NDI software only tracks a single face at a time of a multi-face tool. Each individual face in this case only contained four sphere targets, which makes four the maximum number of usable spheres at any particular position.

The second part of the tracking test resulted in a set of 30 scans such as the four samples shown in Figure 5. The nine disc centroids in each scan were individually determined, and then the 3D standard deviation of the 30 corresponding centroids for each respective disc was calculated and averaged across the 9 discs. This standard deviation was determined to be 1.49 mm.

(a) (b)
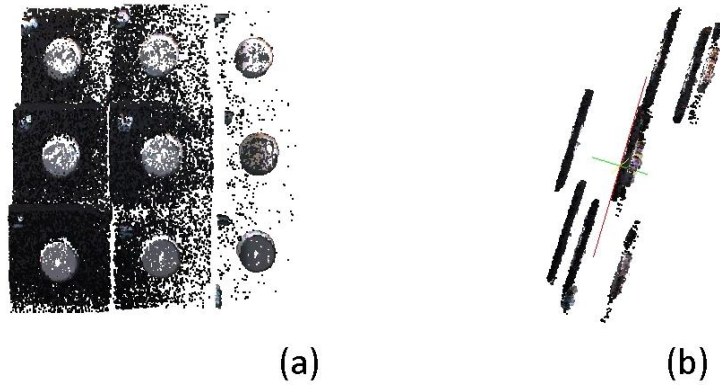
Figure 5. Overlay of representative scans from a single subset of 10 scans (out of 30) taken from the second tracking test, where (a) is a front view and (b) is a side view.

Next, the mean centroid coordinates of the discs were calculated over all 30 scans to generate a single set of nine centroid coordinates which acted as the "gold standard" for the tracking test. The comparison of each subset of 10 scans (10 scans per sphere panel) to this gold standard is shown below in Figure 6. The mean distances of each set of 10 scans to the gold standard 30-scan average were computed, and the three sets of scans were rendered in the same scene and colored according to grouping.

(a) (b)
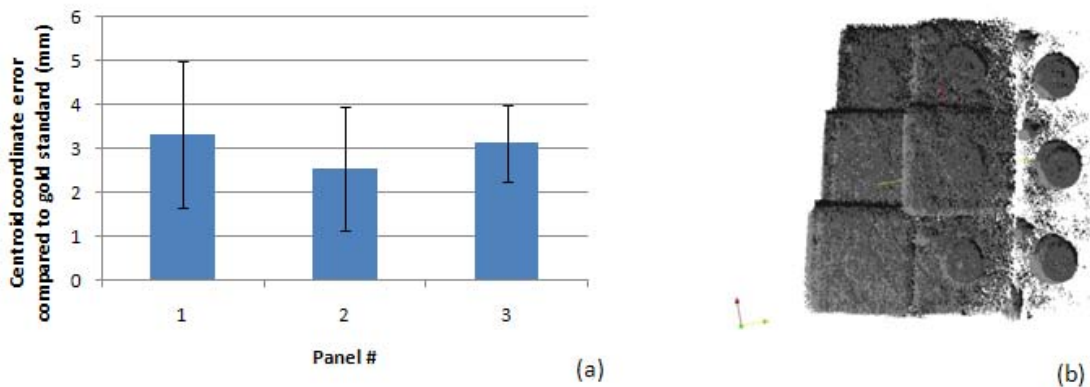
Figure 6. Comparison of the 10 scans taken while tracking each panel (Panel 1 is the rear right panel, Panel 2 is the top panel, and Panel 3 is the rear left panel, looking at the scanner from the rear). The bar graph in (a) shows the average difference between the centroids in the groups of 10 scans compared to the overall 30-scan mean centroids. All 30 scans are rendered in (b), with the lightest gray corresponding to points from Panel 1, the darker gray corresponding to Panel 2, and black corresponding to Panel 3.

5. DISCUSSION AND CONCLUSIONS

The results in Table 1 show that the average geometric scanning error is on the order of half of a millimeter with sub-millimetric standard deviation, which is acceptable for the intended applications of the device. A previous generation LRS using a dual-CCD design was reported by Sinha *et al.* to have a scanning accuracy of 0.3 mm at best, and it was noted that its performance quickly degraded outside of the center of the work volume in part because of error in aligning

the texture and geometric information from their respective CCDs[10]. It is also possible to increase the resolution of the point cloud through the scanner API by collecting more range points, although at the cost of scanning speed.

The sphere visibility results show that on average four spheres were visible to the Polaris in virtually all of the tested positions, providing enough markers to compute the LRS position and orientation. The position at which zero spheres were visible were due to the top of the LRS facing directly away from the Polaris (the sphere panels are located on the rear and top of the LRS) when the scanner is pointed vertically toward the ground. It was important to conduct this test in order to determine limitations in how the LRS may be positioned with regard to the Polaris camera. Equipment positioning in the OR is often beyond the control of the research engineers due to the demands of normal OR logistics, therefore requiring flexibility in the orientation in which the LRS will be tracked. The sphere visibility tests demonstrate that the passive sphere design provides this flexibility.

In addition, the second part of the tracking test determined that the standard deviation in point cloud location when the LRS is tracked from different locations is 1.49 mm, which is on the order of normal optical tracking error. Sinha *et al.* also assessed the tracking ability of the previous generation LRS mentioned above, and found the tracking error to be similar at 1.0 ± 0.5 mm[10]. However, the LRS in that case utilized actively emitting diodes tracked by an NDI Certus camera rather than the passive sphere solution used for the new LRS. The graph in Figure 6a shows that the mean distance to the gold standard centroid locations was on the order of 2.5-3 mm for each of the panel subsets. The standard deviations of the distances to the gold standard were also similar among the three panel subsets, being approximately 1.0-1.5 mm (which is similar to the overall standard deviation calculated from all 30 scans). While it is important to note that the gold standard used in this analysis is not a true gold standard (which would require knowledge of the exact location of the phantom in camera space), it is interesting to note the behavior of the LRS tracking when the different sphere panels are used. There seems to be a slight biasing in the scan locations in camera space depending on the panels used, but within the panel subgroups there is much smaller deviation in the scans. This biasing phenomenon is visible in Figure 6b, represented as the misalignment of the shaded point clouds. This may be due to the averaging of the three calibrations computed from the three panels, and implies that within the OR it is desirable to use the LRS in a consistent orientation relative to the Polaris for all the scans in that particular surgery.

The design goal of a single-lens LRS capable of capturing both geometric and color information was met. It was evaluated with regard to its scanning accuracy and tracking ability using a machined phantom and found to be sufficient for future IGS procedures in the brain and liver. Preliminary guidance tests have been achieved using a liver phantom and its CT images. Work is underway to begin LRS data collection of neurosurgery cases, which will ultimately support development of IGS using model-corrected multi-modal imaging from LRS, MRI, and ultrasound.

REFERENCES

[1]   Nabavi, A., Black, P. M., Gering, D. T., Westin, C. F., Mehta, V., Pergolizzi, R. S., Jr., Ferrant, M., Warfield, S. K., Hata, N., Schwartz, R. B., Wells, W. M., 3rd, Kikinis, R., and Jolesz, F. A., "Serial intraoperative magnetic resonance imaging of brain shift," Neurosurgery **48,** 787-797; discussion 797-788 (2001)
[2]   Nimsky, C., Ganslandt, O., Cerny, S., Hastreiter, P., Greiner, G., and Fahlbusch, R., "Quantification of, visualization of, and compensation for brain shift using intraoperative magnetic resonance imaging," Neurosurgery **47,** 1070-1079; discussion 1079-1080 (2000)
[3]   Nauta, H. J., "Error assessment during "image guided" and "imaging interactive" stereotactic surgery," Comput Med Imaging Graph **18,** 279-287 (1994)
[4]   Sun, H., Roberts, D. W., Farid, H., Wu, Z., Hartov, A., and Paulsen, K. D., "Cortical surface tracking using a stereoscopic operating microscope," Neurosurgery **56,** 86-97; discussion 86-97 (2005)

[5]   Cash, D. M., Sinha, T. K., Chapman, W. C., Terawaki, H., Dawant, B. M., Galloway, R. L., and Miga, M. I., "Incorporation of a laser range scanner into image-guided liver surgery: surface acquisition, registration, and tracking," Med Phys **30,** 1671-1682 (2003)

[6]   Miga, M. I., Sinha, T. K., Cash, D. M., Galloway, R. L., and Weil, R. J., "Cortical surface registration for image-guided neurosurgery using laser-range scanning," IEEE Trans Med Imaging **22,** 973-985 (2003)

[7]   Sinha, T. K., Miga, M. I., Cash, D. M., and Weil, R. J., "Intraoperative cortical surface characterization using laser range scanning: preliminary results," Neurosurgery **59,** ONS368-376; discussion ONS376-367 (2006)

[8]   Cao, A., Thompson, R. C., Dumpuri, P., Dawant, B. M., Galloway, R. L., Ding, S., and Miga, M. I., "Laser range scanning for image-guided neurosurgery: investigation of image-to-physical space registrations," Med Phys **35,** 1593-1605 (2008)

[9]   Cash, D. M., Miga, M. I., Sinha, T. K., Galloway, R. L., and Chapman, W. C., "Compensating for intraoperative soft-tissue deformations using incomplete surface data and finite elements," IEEE Trans Med Imaging **24,** 1479-1491 (2005)

[10]   Sinha, T. K., Dawant, B. M., Duay, V., Cash, D. M., Weil, R. J., Thompson, R. C., Weaver, K. D., and Miga, M. I., "A method to track cortical surface deformations using a laser range scanner," IEEE Trans Med Imaging **24,** 767-781 (2005)

[11]   Ding, S. I., Miga, M. I., Noble, J. H., Cao, A., Dumpuri, P., Thompson, R. C., and Dawant, B. M., "Semiautomatic Registration of Pre- and Postbrain Tumor Resection Laser Range Data: Method and Validation," Ieee Transactions on Biomedical Engineering **56,** 770-780 (2009)